Comparative study of total absorption of light by two-dimensional channel and hole array gratings

Anne-Laure Fehrembach and Evgeny Popov*

Institut Fresnel, CNRS UMR 7249, Aix-Marseille Université, Domaine Universitaire de Saint Jérôme, 13397 Marseille, France

e.popov@fresnel.fr

Abstract: A detailed study of light absorption by silver gratings having two-dimensional periodicity is presented for structures constructed either of channels or of holes with subwavelength dimensions. Rigorous numerical modelling shows a systematic difference between the two structures: hole (cavity) gratings can strongly absorb light provided the cavity is sufficiently deep, when compared to the wavelength, whereas very thin channel gratings can induce total absorption. A detailed analysis is given in the limit when the period tends towards zero, and an explanation of the differences in behavior is presented using the properties of effective optical index of the metamaterial layer that substitutes the periodical structure in the limit when the period tend to zero.

OCIS codes: (050.1950) Diffraction and gratings: Diffraction gratings; (240.6680) Optics at surfaces: Surface plasmons; (260.3910) Physical optics: Metal optics; (050.5745) Diffraction and gratings: Resonance domain.

References and links

1. R. W. Wood, "On a remarkable case of uneven distribution of light in a diffraction grating spectrum," Phylos. Mag. **4**, 396–402 (1902).
2. U. Fano, "The theory of anomalous diffraction gratings and of quasi-stationary waves on metallic surfaces (Sommerfeld's waves)," J. Opt. Soc. Am. **31**(3), 213–222 (1941).
3. M. C. Hutley and D. Maystre, "Total absorption of light by a diffraction grating," Opt. Commun. **19**(3), 431–436 (1976).
4. D. A. Weitz, T. J. Gramila, A. Z. Genack, and J. I. Gersten, "Anomalous low-frequency Raman scattering from rough metal surfaces and the origin of the surface-enhanced Raman scattering," Phys. Rev. Lett. **45**(5), 355–358 (1980).
5. R. Reinisch and M. Nevière, "Electromagnetic theory of diffraction in nonlinear optics and surface enhanced nonlinear optical effects," Phys. Rev. B **28**(4), 1870–1885 (1983).
6. T. W. Ebbesen, H. J. Lezec, H. F. Ghaemi, T. Thio, and P. A. Wolff, "Extraordinary optical transmission through subwavelength hole arrays," Nature **391**(6668), 667–669 (1998).
7. J. Le Perchec, P. Quémerais, A. Barbara, and T. López-Ríos, "Why metallic surfaces with grooves a few nanometers deep and wide may strongly absorb visible light," Phys. Rev. Lett. **100**(6), 066408 (2008).
8. E. Popov, S. Enoch, and N. Bonod, "Absorption of light by extremely shallow metallic gratings: metamaterial behavior," Opt. Express **17**(8), 6770–6781 (2009).
9. R.-L. Chern, Y.-T. Chen, and H.-Y. Lin, "Anomalous optical absorption in metallic gratings with subwavelength slits," Opt. Express **18**(19), 19510–19521 (2010).
10. R. C. McPhedran, G. H. Derrick, and L. C. Botten, "Theory of crossed gratings," in *Electromagnetic Theory of Gratings*, R. Petit, ed. (Springer, Berlin, 1980).
11. L. Li, "Use of Fourier series in the analysis of discontinuous periodic structures," J. Opt. Soc. Am. A **13**, 1870–1876 (1996).
12. L. Li, "New formulation of the Fourier modal method for crossed surface-relief gratings," J. Opt. Soc. Am. A **14**(10), 2758–2767 (1997).
13. M. Nevière and E. Popov, "Crossed gratings," in *Light Propagation in Periodic Media, Differential Theory and Design* (Marcel Dekker, New York, 2003) Chap. 9.
14. M. G. Moharam and T. K. Gaylord, "Rigorous coupled-wave analysis of dielectric surface-relief gratings," J. Opt. Soc. Am. **72**, 1780–1787 (1986).
15. P. Lalanne and G. M. Morris, "Highly improved convergence of the coupled-wave method for TM polarization," J. Opt. Soc. Am. A **13**(4), 779–784 (1996).

#172398 - $15.00 USD Received 11 Jul 2012; revised 21 Aug 2012; accepted 21 Aug 2012; published 6 Sep 2012

16. G. Granet and B. Guizal, "Efficient implementation of the coupled-wave method for metallic lamellar gratings in TM polarization," J. Opt. Soc. Am. A **13**(5), 1019–1023 (1996).
17. J. C. Maxwell-Garnett, "Colors in metal glasses and in. metallic films," Philos. Trans. R. Soc. London Ser. A **203**(359-371), 385–420 (1904).
18. D. Yaghjian, "Electric dyadic Green's functions in the source region," Proc. IEEE **68**(2), 248–263 (1980).
19. G. W. Milton, *The Theory of Composites* (Cambridge Univ. Press, 2002).
20. G. W. Milton and K. Golden, "Representations for the Conductivity Functions of Multicomponent Composites," Commun. Pure Appl. Math. **43**(5), 647–671 (1990).

1. Introduction

Enhanced light absorption by periodic structures has attracted the attention of scientists and engineers since the first observation of grating anomalies by R. Wood [1]. Resonant excitation of surface plasmon waves, responsible for these anomalies was first proposed by Fano [2] as the explication of this phenomenon. Later, Hutley and Maystre [3] have predicted and observed total light absorption (called by them Brewster effect) by relatively shallow gratings, with groove height not exceeding 10% of the wavelength. The resonant excitation of surface plasmons gave explanation to surface-enhanced Raman scattering (SERS) [4] and was largely used in nonlinear optics [5].

Since the work of Ebbesen et al. [6] on the observation of enhanced transmission through metallic hole arrays, surface and volume plasmons became object of so great number of experimental and theoretical studies that gave birth to a new name '*plasmonics'* of the domain.

Light absorption remains also a separate topic of interest for applications in photovoltaics and microwave isolating. Recently, it has been shown that very shallow periodic structures having one- or two-dimensional periodicity can absorb light totally in relatively large spectral and angular interval [7–9]. The advantage of 2D periodicity is the possibility to enhance absorption in unpolarized light, whereas for 1D gratings this is possible by combining surface plasmon and cavity resonances, which imposes tighter constraints to manufacturing.

There are many yet unsolved problems in the theory of periodic structures. A typical example is the study of the similarities and differences between inductive (with continuous perforated metal layer in the grating region) and capacitive grids (where the metal inclusions are separated from each other inside the grating) [10]. Another problem is the choice of homogetization procedure for structures having very small periods when compared with the wavelength of light, structures known as metamaterials.

Our aim in this paper is to study light absorption by two different types of 2D gratings, constructed of channels or holes. If the substrate is dielectric, and the grating bulk material is metal, these systems are called capacitive and inductive grids, respectively [10]. While channel gratings of just several nm depth can absorb light totally, as already shown in [7, 8], the inverted geometry requires much deeper modulation values to obtain similar performance. This difference persists even when the period is reduced to just several nanometers (1/100 of light wavelength). We propose an explanation from metamaterial point of view by testing two approaches for obtaining the formula for the effective dielectric permittivity when the period of the structure tends to zero. A very good agreement is observed between the rigorous electromagnetic modeling and he effective index approach.

2. Comparative study of channel and hole array gratings

Let us consider the reflection properties of silver-made gratings with 2D periodicity, presented schematically in Fig. 1. The first system consists of square pillars separated by channels; the second one contains square holes separated by metallic wall. In what follows, the substrate and the grating material is silver, the wavelength is equal to 457 nm, the cladding, channel and hole material is air. The calculations are done using a rigorous electromagnetic home-made code based on the Fourier Modal Method. Li's factorization rules

#172398 - $15.00 USD Received 11 Jul 2012; revised 21 Aug 2012; accepted 21 Aug 2012; published 6 Sep 2012

[11, 12] are applied for square holes and pillars, and Normal Vector Method [13] is used for circular shapes.

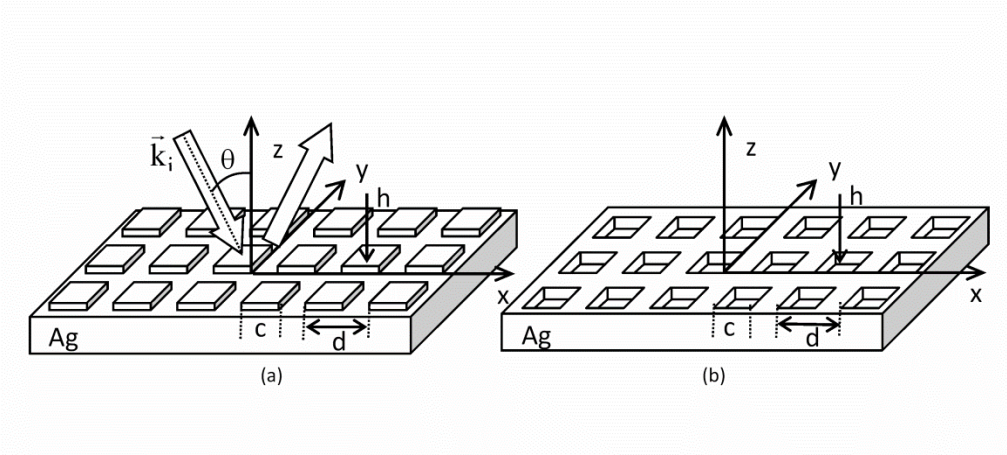

Fig. 1. Schematic representation of two types of gratings having two-dimensional periodicity: (a) channel (capacitive) grating, (b) hole (inductive) grating

The reflection properties of the first system has been studied in [7, 8] and they are characterized by strong absorption in large angular and spectral intervals, even for quite shallow channels. Figure 2(a) gives the dependence of the reflectivity on the channel depth h and the filling ratio f:

$$f = \frac{c^2}{d^2} \tag{1}$$

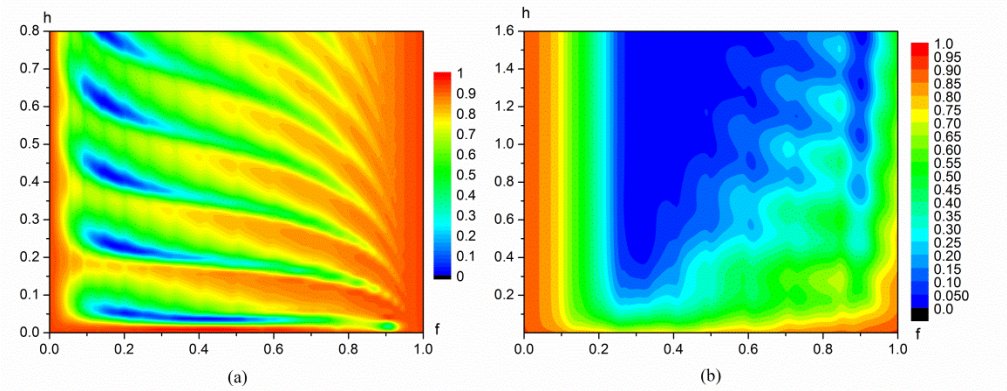

Fig. 2. Reflection of the gratings presented in Figs. 1(a) and 1(b), respectively, as a function of the filing factor f and the channel (hole) depth h (given in μm). Period in x- and y-direction is equal to 250 nm. Wavelength 457 nm in normal incidence.

The period d = 250 nm is chosen to avoid non-specular diffraction orders in the visible. As previously explained [7, 8], these regions of high absorption are due to the metamaterial behavior of the grating structure, which has effective permittivity that is characteristic for highly absorbing anisotropic dielectric, rather than metal (see also next section).On the contrary, the holes grating reflectivity remains highs for shallow holes (Fig. 2(b)), and diminishes significantly only when h > 500 nm. An explanation of this difference between hole and channel gratings, obtained from the metamaterial point of view is discussed in the next section.

#172398 - $15.00 USD Received 11 Jul 2012; revised 21 Aug 2012; accepted 21 Aug 2012; published 6 Sep 2012

There exists a physical explanation for relatively large periods that is linked with the existence of cavity modes inside the channels and the holes, modes that can propagate in the vertical direction. In the case of channels, the fundamental mode has no cut-off for 1D gratings and it is equivalent to the TEM mode in metallic plane waveguides. Figure 3 presents the dependence of the real and imaginary part of the normalized propagation constant of the modes for 2D channel and hole gratings of finite conductivity, taking into account the modal interaction through the channel (or hole) walls by the tunneling effect, and the interaction through the channels open in the perpendicular direction.

The modes are determined by the Fourier-modal expansion of the field inside the grating region, an approach widely known as rigorous coupled-wave (RCW) method. Due to the periodicity of the structure in x- and y-direction, and the invariance in z-direction, the electric field vector in monochromatic regime can be represented in a modal form:

$$\vec{E}(\vec{r}) = \sum_{m,n,p=-\infty}^{\infty} \vec{\varepsilon}_{m,n,p}^{\pm} \exp\left[ik_0 \left(\alpha_m x + \beta_n y \pm \gamma_p z \right) \right] \tag{2}$$

with constant amplitudes $\vec{\varepsilon}_{m,n,p}^{\pm}$, where the sign +/– stands for propagation upward and downward and k_0 is the wavenumber in the superstrate, assumed to be air. If the eigenvalues of the transmission matrix are denoted by $\exp\left(i\gamma_p h\right)$, γ_p are the eigenvalues of the diffraction matrix [11–16] that links the electromagnetic field values with its z-derivatives inside the grating layer. In normal incidence:

$$\begin{aligned} \alpha_m &= m\frac{\lambda}{d_x} \\ \beta_n &= n\frac{\lambda}{d_y} \end{aligned} \tag{3}$$

where λ is the wavelength, and d_x and d_y, the periods in x- and y-direction, respectively.

Because of the invariance of the grating region in z-direction, the mode constants are independent of z. As the filling factor is varied, Fig. 3(a) presents the mode constant having the smallest imaginary part for the channel grating.

In the case of 1D perfectly conducting channels, the TEM mode constant is equal to the refractive index of the channels (equal to one in our case). When f = 0, the pillars in Fig. 1(a) have zero width, so that the fundamental harmonic of the field in Eq. (2) is also equal to one. When the bums are growing in size, the interaction between the modes in the parallel and perpendicular channels leads to increase of the losses (reflected in the increase of the imaginary part of γ).

#172398 - $15.00 USD Received 11 Jul 2012; revised 21 Aug 2012; accepted 21 Aug 2012; published 6 Sep 2012

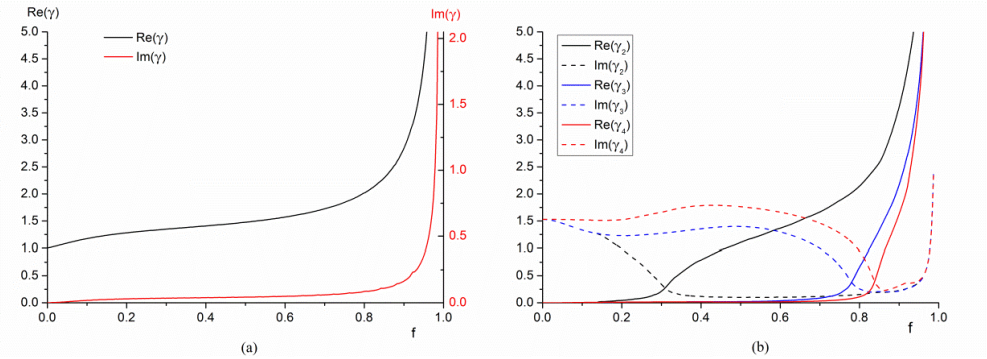

Fig. 3. Real and imaginary parts of the eigenvalues γ of the diffraction matrix, corresponding to Fig. 2(a), as a function of the filling factor. (a) the basic mode with minimum imaginary part; (b) three higher modes.

More interesting is the fact that the real part also grows with f, which can be understood by the fact that the capacitance of the system increases as the gap between the conductive elements decreases. The analysis of the equivalent effective index in the next section for shorter periods shows an increase of the real part of the effective refractive index, which explains the increase of Re(γ).

The existence of this fundamental mode can explain the appearance of consecutive minima and maxima in the reflectivity as a function of h, as well as the decrease of the distance between them as f increases. Indeed, a Fabry-Perot resonance within the grating structure due to the fundamental mode has to be quasiperiodic with respect to h, with the period D_h determined by the real part of the mode propagation constant:

$$D_h = \frac{\lambda}{2\,\mathrm{Re}(\gamma)} \tag{4}$$

For example, when f = 0.6, $D_h \approx 150$ nm in Fig. 2(a), which corresponds to γ = 1.53 in Fig. 3(a).

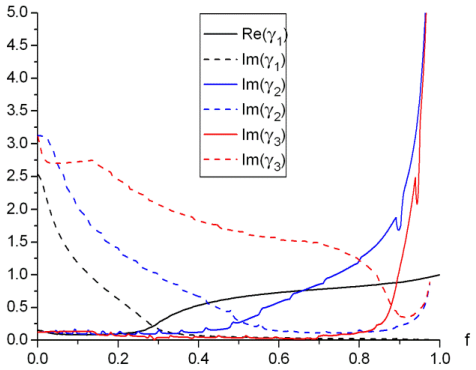

Fig. 4. Real and imaginary parts of the eigenvalues γ of the diffraction matrix, corresponding to Fig. 2(b), as a function of the filling factor.

There are higher modes propagating (and evanescent) inside the structure, as observed in Fig. 3(b) for the next three modes having minimum imaginary part. They are characterized by cut-off filling factor of approximately 0.3, 0.75, 0.85. Contrary to the case of hole grating

#172398 - $15.00 USD Received 11 Jul 2012; revised 21 Aug 2012; accepted 21 Aug 2012; published 6 Sep 2012

(discussed below), we are not able to identify the role of higher modes in the reflectivity behavior in Fig. 2(a), although they definitely participate in the diffraction process. The modal analysis of the hole array grating has been made in detail after the work of Ebbesen [6]. The hole waveguides do not present a TEM mode that has no cut-off. Figure 4 shows that the first mode becomes propagating for f ~0.3, the second one at f ~0.6, the third one at f ~0.85. Each of them leads to well-distinguished anomalies observed in Fig. 2(b), but even their combined role cannot lead to strong light absorption for shallow gratings, contrary to the channel structure.

3. Metamaterial analysis of channel and hole arrays

Since the works of Maxwell-Garnett [17] on the homogenization of Maxwell equations for media with inhomogeneous inclusions, there are numerous theoretical, numerical, and experimental works devoted to the determination of an equivalent effective refractive index (or dielectric permittivity and magnetic permeability in case of magnetic properties of the media) that can replace the "alloy" of different substances involved in the structure. It is difficult here to even mention the most important works. One approach is the so called homogenization technique for periodic media, an approach that analyses the optical properties in the quasistatic regime, when the optical frequency tends to zero. While this is interesting and fruitful approach, it is not quite practical in the near-IR, visible and UV domain, where the optical constants depend strongly on the wavelength. To take into account the dispersion, instead of increasing wavelength to infinity, it is possible to diminish the period(s) to zero. If together with that the grating thickness tends to zero, all effects disappear and the limit becomes a reflection from the substrate-superstrate interface. To avoid this, in what follows, we fix the wavelength and the grating thickness h, and decrease the x-y dimensions.

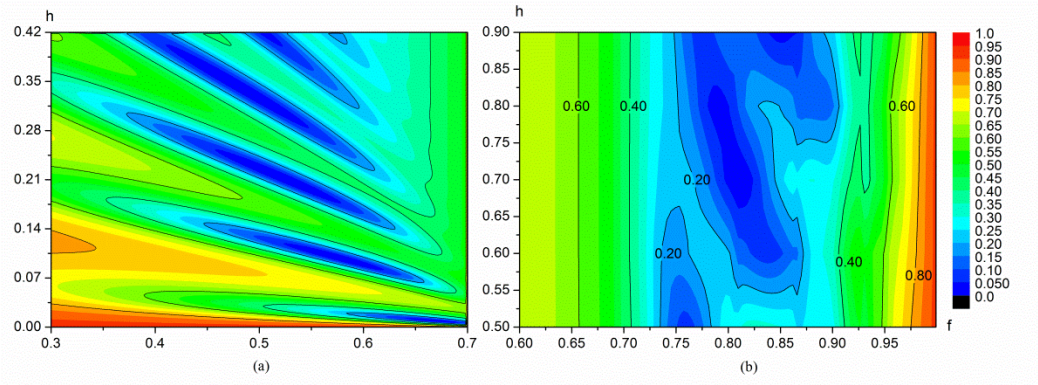

Fig. 5. As in Fig. 2 but for the period of the structures equal to 3 nm (h is again given in μm).

3.1. Numerical results for short periods

The intuitive assumption that the effective permittivity would be the average of the permitivities of the participants fails to be true. The first contra-argument is that it is not clear when to take arithmetic average, when geometric, when some other. The second argument is that the average values for two media are symmetric when the permittivities are mutually permuted, simultaneously with the filling factor.

#172398 - $15.00 USD Received 11 Jul 2012; revised 21 Aug 2012; accepted 21 Aug 2012; published 6 Sep 2012

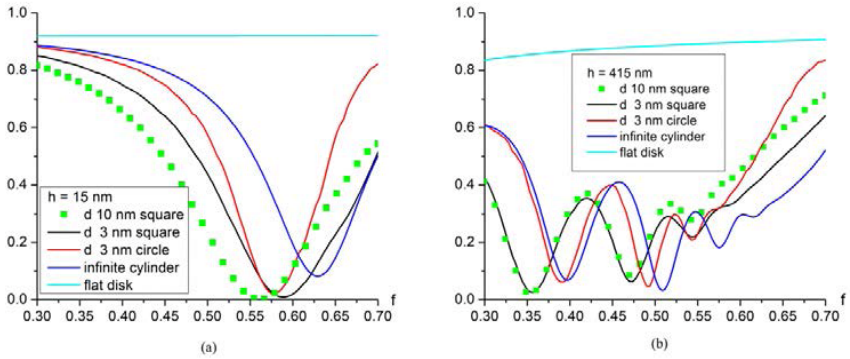

Fig. 6. Reflectivity as a function of the filling factor for the channel grating of Fig. 2(a) for two different periods (10 and 3 nm) and for two different forms of the pillars, square and circuler, as described in the legend. Blue curve, the results of Eqs. (23) and (24), cyan line, Eqs. (25) and (26). (a) h = 15 nm, (b) h = 415 nm.

Numerical results for very small periods, when compared to the wavelength show that the peculiarities in the properties of the gratings, presented in Fig. 3(a) and 3(b) persist, as can be observed in Fig. 5 that shows the dependence of the reflectivity on the filling factor f and grating depth h in the regions of high absorption, obtained by the rigorous numerical method for the two structures of Fig. 1 with period d = 3 nm. In particular, very shallow channel gratings can totally absorb the incident light, which is not the case of hole arrays as seen in Fig. 2(b). Figure 6 shows the dependence on the filling factor of the reflectivity of the grating of Fig. 2(a) for square pillars with period 10 and 3nm, together with a circular pillar reflectivity having period of 3 nm. The grating thickness h is equal to 15 nm (a) and to 415 nm (b). Results obtained for d = 1 nm practically coincide with the results for d = 3 nm. We see that for h = 15 nm the fill-factor dependence of the reflectivity goes down to less than 0.1%, whereas it remains greater than 94.5% for the gratings consisting of circular or square holes. The blue and cyan lines in the figure describe the effective-index results of the effective-index approach, presented further on.

Figure 7 presents similar results of the reflectivity of a square hole arrays for two different hole depths as a function of the filling factor. Similarly to Fig. 6(b), there is no difference between the gratings with periods 3 and 10 nm.

Two conclusions could be drawn from the results:

1) The behavior of very small pitch gratings shows similar peculiarities, independent on the pitch size; the position of the anomalies tends toward a limit position as the period tends to zero. Channel gratings properties differ significantly from the hole arrays whatever small the period is.

2) There is a small difference in Fig. 6 between the gratings consisting of square and circular pillars, the absorption curve for circular pillars is shifted to larger filling factors, as if they seem to have slightly smaller filling factor than the one given by the simple surface ratio in Eq. (1).

#172398 - $15.00 USD Received 11 Jul 2012; revised 21 Aug 2012; accepted 21 Aug 2012; published 6 Sep 2012

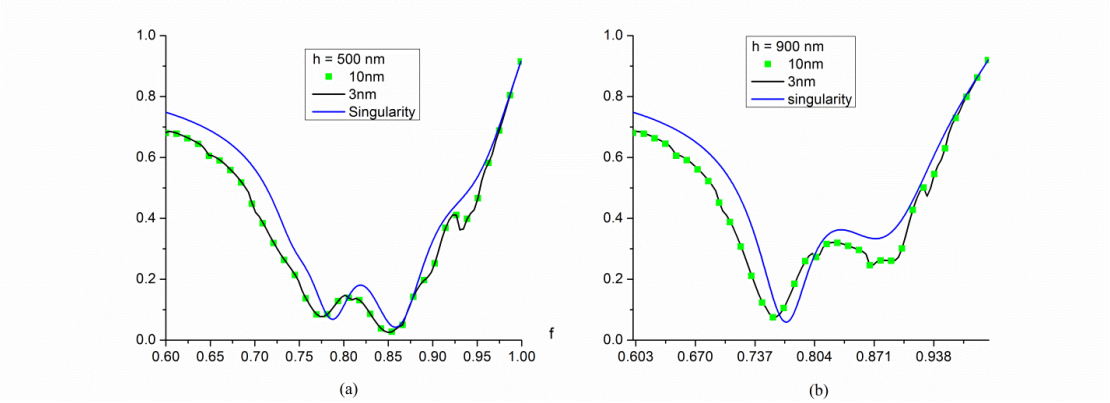

Fig. 7. Reflectivity as a function of the filling factor for the square hole grating of Fig. 2(b) for two different periods (10 and 3 nm), as described in the legend. Blue curve, the results of Eqs. (23) and (24). (a) h = 15 nm, (b) h = 900 nm.

3.2. Equivalent effective-index analysis

In order to obtain a simple model that enables us to better understand the behavior of these short-pitch structures, we use an effective-index approach based on the Maxwell-Garnett approach [17] and Green tensor singularity analysis [18].

Let us consider at first the Green's function approach to light scattering by an object having permittivity ε_2 embedded in a medium with permittivity ε_1. The incident field $\vec{E}_i(\vec{r})$ will create a total field $\vec{E}(\vec{r})$, which is a sum of the incident and the scattered field:

$$\vec{E}(\vec{r}) = \vec{E}_i(\vec{r}) + \int_{scatterers} \mathbf{G}(\vec{r}-\vec{r}')\left(\frac{\varepsilon_2}{\varepsilon_1}-1\right)\vec{E}(\vec{r}')\,d\vec{r}' \tag{5}$$

The latter depends on the total field all over the scattering object through the electric dyadic Green's tensor **G**. This tensor has a singular **L** and a principal value $\mathbf{P}_v$ parts:

$$\mathbf{G}(\vec{r}-\vec{r}') = \mathbf{L}\,\delta(\vec{r}-\vec{r}') + \mathbf{P}_v G(\vec{r}-\vec{r}') \tag{6}$$

where $\delta(\vec{r}-\vec{r}')$ is the Dirac function. In the first order approximation, the strongest contribution is the auto-scattering part expressed by the singular part of the Green's function:

$$\vec{E}(\vec{r}) \approx \vec{E}_i(\vec{r}) + \mathbf{L}\left(\frac{\varepsilon_2}{\varepsilon_1}-1\right)\vec{E}(\vec{r}) \tag{7}$$

wherefrom:

$$\vec{E}(\vec{r}) \approx \left[\mathbf{1} - \mathbf{L}\left(\frac{\varepsilon_2}{\varepsilon_1}-1\right)\right]^{-1}\vec{E}_i(\vec{r}) \tag{8}$$

where bold one stands for the tree-dimensional unit tensor. The trace of L must be equal to one [18]:

$$Trace(\mathbf{L}) = 1 \tag{9}$$

The singular part has a simple form and depends on the form of the object. A detailed analysis and many examples can be found in ref.17. In particular, for a sphere or a cube:

#172398 - $15.00 USD Received 11 Jul 2012; revised 21 Aug 2012; accepted 21 Aug 2012; published 6 Sep 2012

$$\mathbf{L} = -\begin{pmatrix} 1/3 & 0 & 0 \\ 0 & 1/3 & 0 \\ 0 & 0 & 1/3 \end{pmatrix} \tag{10}$$

and for long cylindrical inclusions with circular or square cross-section having axis along z-direction:

$$\mathbf{L} = -\begin{pmatrix} 1/2 & 0 & 0 \\ 0 & 1/2 & 0 \\ 0 & 0 & 0 \end{pmatrix} \tag{11}$$

Equations (8) and (10) permit immediately to obtain the well-known electric response of a spherical inclusion (or cavity):

$$\vec{E}(\vec{r}) \approx \frac{3\varepsilon_1}{2\varepsilon_1 + \varepsilon_2} \vec{E}_i(\vec{r}) \tag{12}$$

For our needs, we shall at first consider as if the grating layer is extended infinitely in z-direction, in order to obtain its effective permittivity. Using Eqs. (8) and (11), the link between the scattered and the incident field is given as:

$$\vec{E}(\vec{r}) \approx \begin{pmatrix} \frac{2\varepsilon_1}{\varepsilon_1 + \varepsilon_2} & 0 & 0 \\ 0 & \frac{2\varepsilon_1}{\varepsilon_1 + \varepsilon_2} & 0 \\ 0 & 0 & 1 \end{pmatrix} \vec{E}_i(\vec{r}) \tag{13}$$

There are some doubts whether the choice of the geometry (infinitely long cylinders) is the good one, because for thin gratings probably more suitable is to consider the inclusions as thin discs. If the height of the disk is much smaller than its cross-section width, the singularity of the Green's function tensor takes the form:

$$\mathbf{L} = -\begin{pmatrix} 0 & 0 & 0 \\ 0 & 0 & 0 \\ 0 & 0 & 1 \end{pmatrix} \tag{14}$$

And the link between the total and the incident field takes the following form:

$$\vec{E}(\vec{r}) \approx \begin{pmatrix} 1 & 0 & 0 \\ 0 & 1 & 0 \\ 0 & 0 & \frac{\varepsilon_1}{\varepsilon_2} \end{pmatrix} \vec{E}_i(\vec{r}) \tag{15}$$

The tensor establishing the link in Eqs. (13) and (15) is denoted as **Q**. In what follows, numerical study will distinguish the choice between Eqs. (13) and (15).

The original approach proposed by Maxwell-Garnett [17] enables us to find the effective permittivity ε_{eff} of the inhomogeneous medium, based on a simple hypothesis that it gives the link between the mean values of electric and displacement fields:

#172398 - $15.00 USD Received 11 Jul 2012; revised 21 Aug 2012; accepted 21 Aug 2012; published 6 Sep 2012

$$\left\langle \vec{D} \right\rangle = \varepsilon_{eff} \left\langle \vec{E} \right\rangle \tag{16}$$

where angular brackets stand for mean value and, in general, ε_{eff} is a tensor. On the other hand, in the first-order approximation, inside the inclusions the electric field is equal to the total field $\vec{E}(\vec{r})$, whereas outside the inclusions it is equal to $\vec{E}_i(\vec{r})$, so that its mean value is given as:

$$\left\langle \vec{E} \right\rangle = f\ \vec{E}(\vec{r}) + (1-f)\vec{E}_i(\vec{r}) \tag{17}$$

In the same manner:

$$\left\langle \vec{D} \right\rangle = f\ \vec{D}(\vec{r}) + (1-f)\vec{D}_i(\vec{r}) \tag{18}$$

where $\vec{D}_i(\vec{r})$ is the displacement outside the inclusions, and $\vec{D}(\vec{r})$ - inside them. On the other hand, from the macroscopic Maxwell equation we have the two standard relations:

$$\begin{aligned} \vec{D}(\vec{r}) &= \varepsilon_2 \vec{E}(\vec{r}) \\ \vec{D}_i(\vec{r}) &= \varepsilon_1 \vec{E}_i(\vec{r}) \end{aligned} \tag{19}$$

Substitution of Eqs. (17)-(19) into Eq. (16) results in the following relation:

$$f(\varepsilon_{eff} - \varepsilon_2)\vec{E}(\vec{r}) = -(1-f)(\varepsilon_{eff} - \varepsilon_1)\vec{E}_i(\vec{r}) \tag{20}$$

Taking into account that $\vec{E}(\vec{r}) = \mathbf{Q}\ \vec{E}_i(\vec{r})$, the tensor ε_{eff} takes the form

$$\varepsilon_{eff} = \left[(1-f)\ \varepsilon_1 + f\ \mathbf{Q}\ \varepsilon_2\right]\left[1 - f(\mathbf{1} - \mathbf{Q})\right]^{-1} \tag{21}$$

In the case of electrically isotropic media, ε_1 and ε_2 are scalars. In addition, in the case of highly symmetrical inclusions, the **Q** tensor is diagonal (see above), Eq. (21) is simplified into:

$$\varepsilon_{eff,ii} = \frac{(1-f)\ \varepsilon_1 + f\ Q_{ii}\ \varepsilon_2}{1 - f(1 - Q_{ii})}, \quad i = x, y, z \tag{22}$$

A well-known conclusion implies that a mixture of isotropic substances lead to anisotropic effective permittivity. Less obvious is the observation that the exchange of both ε_1 with ε_2 and f with (1 – f) does not keep the result for ε_{eff} the same. In particular, considering long cylindrical inclusions, as described by Eqs. (11) and (13), the effective permittivity represent anisotropic uniaxial medium with axis along the cylinder axis. The ordinary part of the permittivity (in the x-y plane) is given by:

$$\varepsilon_{eff,xx} = \varepsilon_{eff,yy} = \varepsilon_{eff,o} = \varepsilon_1 \frac{(1+f)\ \varepsilon_2 + (1-f)\ \varepsilon_1}{(1-f)\ \varepsilon_2 + (1+f)\ \varepsilon_1} \tag{23}$$

While the extraordinary part along the z-axis represents the mean arithmetic value of the two permittivities:

$$\varepsilon_{eff,zz} = \varepsilon_{eff,e} = f\ \varepsilon_2 + (1-f)\ \varepsilon_1 \tag{24}$$

If, instead of long object, we consider flat ones, Eqs. (14) and (15), the resulting tensor of effective permittivity is also uniaxial, but it contains the mean arithmethic value of the two permittivities in the x-y plane:

#172398 - $15.00 USD Received 11 Jul 2012; revised 21 Aug 2012; accepted 21 Aug 2012; published 6 Sep 2012

$$\varepsilon_{eff,xx} = \varepsilon_{eff,yy} = \varepsilon_{eff,o} = f\,\varepsilon_2 + (1-f)\,\varepsilon_1 \tag{25}$$

While along the z-axis we obtain the mean harmonic value:

$$\varepsilon_{eff,zz} = \varepsilon_{eff,e} = \frac{\varepsilon_1 \varepsilon_2}{f\,\varepsilon_1 + (1-f)\,\varepsilon_2} \tag{26}$$

There are two arguments to choose the first approach (the singularity of infinitely long cylinder. First, when the unit cell cross-section tends to zero with the reduction of the periods and keeping the thickness h fixed, the cross-section diameter can become infinitely smaller than h. Second, Eqs. (25) and (26) are symmetrical when permuting ε_2 *and* ε_1 simultaneously with f *and* $(1-f)$, i.e., channel and hole gratings would be equivalent by interchanging f to 1-f, which is not the case.

If we go back to Fig. 6, the results using the two approaches are presented in blue (for infinitely long cylinders) and cyan (infinitely thin disks). As can be expected, the first approach, Eqs. (23) and (24), gives much better results, which are quite close to the numerical values for circular pillars.

Similar correspondence between the results of the effective-index approach and the numerical method are observed in Fig. 7 for cavity resonances.

The main disadvantage of this simplified approach is that the results depend only on the filling factor, while not taking into account the form of the cross-section of the pillars or holes, while numerical results given in Fig. 6 show that there is a slight difference in the position of the reflectivity dip for circular and square cross-sections. In order to take into account the cross-section form, it is necessary to use more sophisticated approaches that have been developed during the last 120 years. An interested reader can find a detailed work on homogenization theory in a recent review by G. W. Milton [19]. The specific form can be taken into account by the concept of polarisability, and the necessity to use the average values not only of the fields but of the modulus square of the electric field (see ch.16 of [19] and ref [20].). However, we are not able to directly apply this approach, because it is developed in the quasistatic limit as the frequency tends to zero, while in our case the frequency is finite, and the periods in the grating plane tend to zero.

4. Single-mode model and effective index behavior

This quite good correspondence between the rigorous numerical results and the metamaterial approximation enables us to obtain a deeper insight in the origin of the strong light absorption, as well as of the difference between channel and hole structures. Similar to Fig. 2, well-designed regions of low reflectivity are observed, pointing toward some type of modal structure for d = 3 nm in Fig. 5. This can be observed in detail in Fig. 8 that presents the results of the metamaterial behavior of the two structures in Fig. 1 by using Eqs. (23) and (24) to model the grating region, i.e., the structures are represented as a homogeneous anisotropic layer deposited on a metallic substrate. The square regions bordered by black lines in the figure correspond to the scale limits of Figs. 5(a) and 5(b).

#172398 - $15.00 USD Received 11 Jul 2012; revised 21 Aug 2012; accepted 21 Aug 2012; published 6 Sep 2012

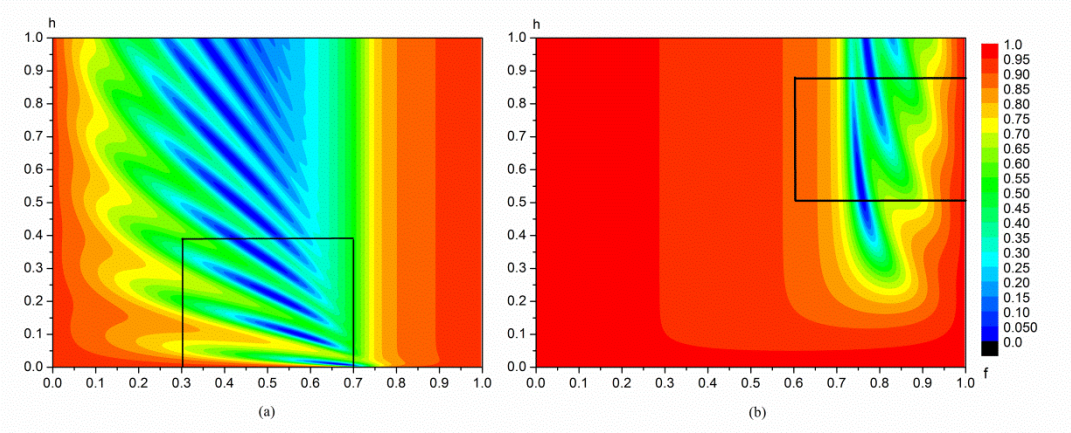

Fig. 8. Reflectivity as a function of f and h of metamaterial layers on silver substrate, corresponding to the limit of structures given in Fig. 2 when the period of the structures tends to zero. (a) channel grating, (b) hole array.

In normal incidence, the normalized propagation constant of the waves propagating in direction to +/– z is equal to the effective refractive index in direction x for the waves polarized in y. The values of $n_{eff,xx}$ are given in Fig. 9. For the channel gratings, as f increases, the real part of the effective index (and thus the real part of the normalized propagation constant of the vertical mode) increases, which explains why the distance in h of the resonances in Fig. 8(a) decreases with h (see Eq. (4)). In fact, for f < 0.7, the metamaterial behaves like a lossy dielectric with large optical index, having real part that varies from 1 to 6. The same behavior was observed for d = 250 nm in sec.1. As f approaches 0.7, both real and imaginary part grow significantly, thus a very thin optical layer (several nanometers thick) can totally absorb the incident light.

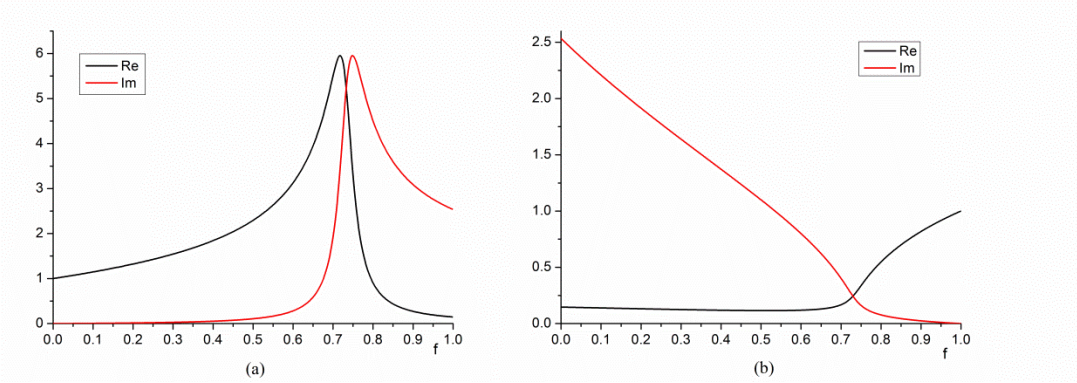

Fig. 9. Dependence on the filling factor f of the real and imaginary parts of the normalized propagation constant of the wave propagating in direction of z, equal to $n_{eff,xx} = \sqrt{\varepsilon_{eff,xx} / \varepsilon_0}$. (a) channel grating, (b) hole array.

When the channel width decreases (f > 0.7), the effective medium is transferred into a lossy metal, with optical properties tending towards the properties of the metal of the pillar.

Let us consider now the case of hole gratings. When the holes cover completely the grating region (f = 1), the modulated layer is air. Reducing the hole size, the real part of the effective index decreases, in contrast with Fig. 9(a). The other important fact is the small increase of its imaginary part, as compared with Fig. 9(a). Close to the cut-off of the mode

#172398 - $15.00 USD Received 11 Jul 2012; revised 21 Aug 2012; accepted 21 Aug 2012; published 6 Sep 2012

near f = 0.7, both the real and the imaginary parts remain small, which fact explains why for small values of h there is no strong absorption, as seen in Fig. 8(b).

Conclusions

As already observed in [7–9], the reflection properties of subwavelength two-dimensional grating depend significantly on the form of the structure. When it consists of pillars separated by channels, there exists a fundamental mode that propagates in vertical direction due to the field interaction through the channels, even for narrow channels, with width less than 5% of the light wavelength. Due to the existence of this mode, the grating structure behaves like a lossy high-index anisotropic dielectric, with characteristic Fabry-Perot resonances observed as a function of its thickness. For channels narrower than 5%, this fundamental mode becomes evanescent and the structure behaves like lossy metal. Close to the cut-off, due to the very high losses and large real part of the effective index, one can observe total light absorption by the layer having thickness of the order of 10 nm.

The corresponding structure that consists of hole instead of pillars is characterized by a vertical mode that has a cut-off (fact well known for single apertures and periodical hole arrays). When propagating, its real part is smaller than unity; this is why strong light absorption and Fabry-Perot resonances appear for thicknesses comparable to the wavelength of light.

These conclusions are also valid in the limit as the structure periods in both x- and y-directions tend toward zero, as shown numerically. A simple Maxwell-Garnett homogenization approach gives very good coincidence with the rigorous numerical results. An open question remains to explain the small difference between the numerical results for circular and square-form pillars, difference that cannot be explained using effective-index approximation that depends only on the filling factor.

#172398 - $15.00 USD Received 11 Jul 2012; revised 21 Aug 2012; accepted 21 Aug 2012; published 6 Sep 2012